Journal of Membrane Science 492 (2015) 439–451

Contents lists available at ScienceDirect

Journal of Membrane Science

journal homepage: www.elsevier.com/locate/memsci

Preparation and sintering behaviour of $La_{5.4}WO_{12-\delta}$ asymmetric membranes with optimised microstructure for hydrogen separation

Wendelin Deibert [a,b,*], Mariya E. Ivanova [a,b,**], Wilhelm A. Meulenberg [a,b], Robert Vaßen [a,b], Olivier Guillon [a,b]

[a] Forschungszentrum Jülich GmbH, Institute of Energy and Climate Research, Materials Synthesis and Processing (IEK-1), Leo-Brandt-Str., D-52425 Jülich, Germany
[b] Jülich Aachen Research Alliance: JARA-Energy

ARTICLE INFO

Article history:
Received 13 February 2015
Received in revised form
28 April 2015
Accepted 31 May 2015
Available online 9 June 2015

Keywords:
Hydrogen separation
Ceramic membranes
Proton–electron mixed conducting ceramics
Lanthanum tungstate
Tape casting

ABSTRACT

$La_{5.4}WO_{12-\delta}$ (LaWO) is a promising membrane candidate for a variety of H_2-related applications due to its appreciable levels of mixed proton–electron conduction and its stability in moist reducing atmospheres at elevated temperatures. Governed by Wagner theory, the H_2 permeation performance of a membrane can be enhanced by reducing its thickness. Therefore, the present work deals with preparing LaWO supported membranes with reduced thickness and optimised microstructure. Combining a dense membrane with a porous supporting layer is associated with mismatched sintering rates, which ultimately lead to bending effects. Therefore, the sintering behaviour of both the dense membrane and the porous substrate must be carefully adjusted to each other. For this purpose, single and co-fired membrane and substrate layers were produced by tape casting. Sintering experiments were carried out with an optical dilatometer. The shrinkage and microstructural evolution of the layers were evaluated in terms of the anisotropic shrinkage forces and the membrane rigidness counteracting the substrate shrinkage. The results were used to develop asymmetric LaWO membranes with optimal microstructure. High membrane density was combined with a substrate porosity of ~30% and minimised bending (40 μm). The LaWO membrane–substrate assembly displayed a He leakage of 10^{-5} hPa dm³ cm^{-2} s^{-1}, which is a value that satisfies further practical demands.

1. Introduction

Hydrogen has the potential to be employed as a high-efficiency fuel in a variety of mobile and chemical systems as well as in the IGCC power plant concept, which is an alternative to conventional fossil fuel power plants. High-purity H_2 can be supplied to fuel cells, chemical reactors, combustion engines, and gas turbines, and only releases water vapour as an exhaust gas [1,2].

The transformation of hydrocarbons, e.g. from coal or biomass, into H_2 is feasible by gasification upon addition of water vapour and O_2. The resulting syngas $CO+H_2$ is then transformed to CO_2+H_2 upon further addition of water in the water-gas shift reaction (WGSR; low temperature shift at 190–230 °C and high temperature shift at 300–360 °C). One method of increasing the overall process efficiency by reducing the heat losses resulting from the large temperature difference between gasification and WGSR is to boost the WGSR to high temperatures (600–900 °C) by continuously removing hydrogen from the product side. The combination of the WGSR with continuous H_2 removal has the unique advantage of allowing the WGSR to be carried out at temperatures that would otherwise be unfavourable for an exothermic reaction in equilibrium. For this purpose, the integration of a high-performance H_2 permeation ceramic membrane (in the WGSR, reactors for combined chemicals and energy production, and pre-combustion IGCC) represents a very promising but challenging possibility [3].

In this context, the main requirements for a potential ceramic membrane material are an appreciable mixed proton and electron conductivity, thermal and hydrothermal stability, as well as chemical stability in reducing and water-containing atmospheres (CO_2, CO, H_2, H_2O, H_2S) at elevated temperatures.

In the last few decades, a number of ceramic materials from different structural classes have been considered as possible candidates for ceramic membranes in H_2-separation applications. Due to the highest levels of proton–electron conductivity exhibited

* Corresponding author at: Forschungszentrum Jülich GmbH, Institute of Energy and Climate Research, Materials Synthesis and Processing (IEK-1), Leo-Brandt-Str., D-52425 Jülich, Germany. Tel.: +49 2461 61 8968; fax: +49 2461 61 2455.
** Corresponding author at: Forschungszentrum Jülich GmbH, Institute of Energy and Climate Research, Materials Synthesis and Processing (IEK-1), Leo-Brandt-Str., D-52425 Jülich, Germany. Tel.: +49 2461 61 5194; fax: +49 2461 61 2455.
E-mail addresses: w.deibert@fz-juelich.de (W. Deibert), m.ivanova@fz-juelich.de (M.E. Ivanova).

http://dx.doi.org/10.1016/j.memsci.2015.05.065

by the acceptor-doped cerates and zirconates, these materials of perovskite structure have continuously been the focus of research for H_2-related applications[2,4–8]. However, the main disadvantage of perovskite structure materials containing alkaline earth metals [6], particularly cerates, is their low stability in CO_2, H_2O and S-containing atmospheres. Although zirconates remain stable under reducing atmospheres, their inherently low grain-boundary conductivity and extreme sintering temperatures significantly limit their practical applications unless sophisticated interface engineering and non-conventional manufacturing approaches are considered. Other proton-conducting ceramic materials, such as the rare-earth sesquioxides (Tb_2O_3) [9], pyrochlores like $La_2Zr_2O_7$ [10] and a number of acceptor-doped niobates [11–14], exhibit conductivity levels that are rather low for realistic H_2-separation membrane applications in spite of their pronounced chemical stability.

In the last few years, much attention has been dedicated to $La_{6-x}WO_{12-\delta}$ (LaWO) from the class of defective fluorites. This is a very promising membrane material fulfilling the above-mentioned requirements. However, this material has not yet been investigated in all facets, particularly in terms of certain practical issues associated with asymmetric membrane preparation, which is the focus of the present work.

$La_{5.8}WO_{12}$ (LaWO) was first reported by Shimura et al. to exhibit a total conductivity in the order of $5{\bullet}10^{-2}$ S/cm at 800 °C in wet H_2 [15]. Since then, LaWO in pure [16] [17] and substituted form (Nd_5LaWO_{12}, $(La_{5/6}Nd_{1/6})_{5.5}WO_{12-\delta}$) [17]–[19], as well as other rare-earth (RE) tungstate materials with lower crystallographic symmetry (Er_6WO_{12}, Nd_6WO_{12}, Eu_6WO_{12}) [20–22], have been subjected to intensive study. Apart from a rather limited number of substituted REWO (with e.g. Mo, Re), for which a conductivity improvement could be ascertained [20] [17], LaWO remains the major membrane candidate amongst the REWO materials due to its high structural symmetry (cubic) and the resulting thermodynamic stability of proton defects up to high temperatures (about 800 °C). In the present work, we will consider the case of non-substituted LaWO, and investigate its properties in more detail.

Significant proton conductivity was ascertained for LaWO in [23,24] by demonstrating an isotope effect. Protons are the dominating charge carriers in LaWO at temperatures up to about 600 °C [16]. When the temperature is increased, oxygen ionic and electronic charges also start contributing to the overall electrical behaviour of this material. At about 800 °C, electronic conduction becomes the dominant process, while proton conductivity decays due to dehydration of the material.

The bulk transport of H_2 in the LaWO material results from the simultaneous diffusion of protons and electrons through the crystal lattice, governed in general by the H_2 activity gradient. Therefore, the proper operating regime of a LaWO membrane for H_2 separation is in the temperature range of 600–800 °C, where the protons remain stable in the structure and a sufficient electron contribution is present as well. Proton transport through such a bulk membrane is described by Wagner transport theory [14], Eq. (1):

$$j_{H^+} = \frac{-RT}{2F^2L}\int_I^{II}(\sigma_{e^-}\ t_{H^+})\, d\ln p_{H_2} \quad (1)$$

where j_{H^+} is the proton flux; R is the universal gas constant; F is the Faraday constant; L is the membrane thickness; σ_{e^-} is the electronic conductivity; t_{H^+} is the proton transport number; p_{H_2} is the hydrogen partial pressure.

The analysis of this equation allows the identification of different strategies to improve the membrane's H_2 transport properties, namely by means of (i) optimisation of material properties (σ_{e^-} and t_{H^+} terms in Eq. (1)), (ii) selection of optimal operation parameters (grad p_{H_2}, operating T), and (iii) membrane architecture (to reduce the membrane thickness L).

These three strategies are considered briefly below with respect to LaWO.

1.1. Optimisation of material properties

The LaWO membrane itself can be operated in a certain LaWO single-phase range (e.g. 5.3–5.7 at 1500 °C [25] and from 5.2 to 5.5 [17] at 1300–1500 °C), strictly excluding the presence of non-reacted or segregated La_2O_3 as well as the formation of the secondary phase $La_6W_2O_{15}$. These two secondary phases are well known for their negative impact, causing a decreased mechanical stability and material performance of LaWO-based membranes [26].

In recent years, the realistic crystallographic structure of LaWO was illuminated and the actual LaWO composition was formulated as $La_{6.63}W_{1.17}O_{13.43}$ (La/W ratio of 5.6) in [25] or $La_{28-x}W_{4+x}O_{54+\delta\nu/2-\delta}$ in [27], where ν stands for oxygen vacancies and x represents the amount of W dissolved on the La sites. It thus became clear that the single-phase LaWO material could only be obtained within a certain W over-stoichiometry window. This is closely related to the defect chemistry of LaWO material, e.g. the defect interactions within the crystal structure. A detailed defect structure model was discussed in [28]. In brief, a W(6+) cation residing on a La(3+) site represents a donor defect of (3+) effective charge. The presence of such donor defects maintains the O(2−) concentration at fixed levels to achieve electroneutrality. This results in sufficient structural stability of the LaWO material at the expense of slightly decreased electrical conductivity, as shown in [25].

On the other hand, LaWO can be optimised for maximum proton and electron conductivity and a resulting increased H_2 flux via the addition of acceptor substitutions and metal cations with variable valence, as shown in [17,29]. The W substitution by cations of similar ionic radii and electronegativities, as well as cations of mixed valence, represents a solution for improving the thermodynamic stability of the protons and simultaneously achieving appreciable levels of electronic defects. This will ultimately lead to an expansion of the material operational window to broader temperature and partial pressures ranges.

These considerations are reflected in the case of Re- and Mo-substituted REWOs, leading to significantly increased H_2 permeation rates compared to the nominally non-substituted compounds, as demonstrated first by Serra [20]. The H_2 flux measured on bulk 900 μm-thick $La_{5.5}WO_{12-\delta}$ membranes in a dry/wet configuration (dry H_2–He feed and wet Ar sweep with $pH_2O = 0.025$ atm) was about 0.06 ml min^{-1} cm^{-2} at 900 °C [30,29]. $La_{5.5}W_{0.8}Re_{0.2}O_{11.25-d}$ with a thickness of 760 μm showed a permeation rate of 0.095 ml min^{-1} cm^{-2} at 700 °C in dry/wet configuration with the same gas conditions as mentioned for the pure LaWO [29]. Comparable permeation rates were reached at temperatures that were lower by 200 °C with the substituted material [29].

1.2. Selection of optimal operation parameters

As outlined above, in relation to the Wagner equation, the temperature and applied pressure across the membrane are the two operation-related parameters. They represent the diffusion-activating parameter (T) and the driving force for H_2 diffusion across the bulk (grad p_{H_2}), respectively. These parameters depend on the targeted process, in which the membrane will be integrated. As previously mentioned, the optimal operation temperatures for LaWO are within the range of 600–800 °C due to the thermodynamic instabilities of proton defects at higher temperatures. Therefore, operating temperatures higher than 800 °C are

not feasible. To achieve higher H_2 flux values, the partial pressure gradient can be increased. Combined with the membrane sealing process, this challenges the integrity and mechanical stability of the membrane. In this context, the mechanical properties of LaWO are very important with respect to its potential application in e.g. membrane modules for hydrogen production. The mechanical properties of LaWO were characterised in [31], where hardness (8–9 GPa), Young's modulus (130 ± 15 GPa), and fracture toughness (2 MPa $m^{1/2}$) were determined [31]. The values reported for LaWO were slightly lower than for other potential membrane materials for hydrogen separation, e.g. $BaZrO_3$ with a Young's modulus of 181 ± 11 GPa and hardness of 11.1 ± 1.9 GPa [32].

1.3. Membrane architecture

The geometry-related parameter in Eq. (1) is represented by the thickness of the membrane, which can be reduced by advanced manufacturing methods so that the final architecture provides sufficient mechanical stability and durability for μm-thick membranes. The preparation of stable and defect-free LaWO membranes with an optimal architecture poses a serious challenge. Only an extremely limited number of studies have reported so far on the performance of asymmetric LaWO membranes. In [33], a H_2 flux of 0.04 $ml \cdot min^{-1} cm^{-2}$ was demonstrated at 900 °C in humid (2.5 vol% H_2O) atmosphere with 9.75 vol% H_2 for an asymmetric membrane with a thickness of 25–30 μm with a substrate made from the same material.

One of the most critical issues when membrane thickness is reduced is the loss of mechanical stability. Therefore, an asymmetric membrane assembly consisting of a dense membrane layer and a porous substrate must be engineered as described elsewhere [34]. Membrane structures with a thickness between 10 and 30 μm require a mechanical support to withstand the stresses during the sealing and operation processes but this support must also have sufficient porosity (30–40%) to ensure optimal gas supply. Combining a gas-tight membrane layer with a porous supporting layer evokes a variety of fabrication issues, such as anisotropic shrinkage and bending effects, which are interrelated. Solving these issues is the key to obtaining reproducible and flat asymmetric membrane architectures. Therefore, a detailed analysis is essential to enable the necessary optimisation of asymmetric LaWO membranes with a view to upscaling them and integrating them as system components.

A convenient manufacturing method is needed to produce a defect-free membrane (no cracks, pin-holes) with reduced thickness in the μm range. Different approaches have been reported for such membrane architectures. A colloidal processing route [35], pressing [36,37], or a combination of tape casting and lamination [38] represent options for creating stable membrane designs. The resulting LaWO tapes reported by Weirich et al. had a total thickness of 300 μm, a membrane thickness of 40 μm and consisted of the same material for both layers. Carbon black was added to the substrate layer to adjust the porosity [38].

In the present paper, the selected technique was sequential tape casting, which has already been used for the fabrication of components for solid oxide fuel cells [39]·[40] as well as oxygen separation membranes [39–42], capacitors [43], and microelectronics [44,45]. Tape casting is a well-established process for the fabrication of large-area ceramic sheets [46]. The typical thickness of the tape-cast components ranges between a few μm to about 1 mm [46] depending on the tape-casting device. The main advantage of this technology is its high automation and proximity to industrial-scale applications.

Another critical point is the chemical and thermal compatibility between the substrate and membrane materials. In earlier studies, we investigated the chemical compatibility of LaWO with selected materials which are used as state-of-the-art substrates in SOFC development (Table 1). We also investigated the thermal compatibility of LaWO with different substrate material candidates in membrane development [13]. With both Y_2O_3-stabilised ZrO_2 (YSZ) and NiO, LaWO reacts readily at elevated temperatures. The application of SOFC standard substrate material YSZ:NiO is not suitable for LaWO membrane development at temperatures of 1100 °C and higher. At lower temperatures (e.g. 600–800 °C), at which the two materials do not react, the application of a gas-tight supported membrane is practically unrealisable due to the high sintering temperatures of LaWO. As Table 1 indicates, a possible substrate material is Gd_2O_3-doped CeO_2 (CGO), but as demonstrated in [13], the thermal expansions of LaWO ($\alpha = 11*10^{-6} K^{-1}$) and this substrate material ($\alpha = 14*10^{-6} K^{-1}$) differ considerably at temperatures above 800 °C. This rules out the practical application of CGO as a substrate material in LaWO membrane development.

Based on these considerations, LaWO was therefore selected as an optimal option for fabrication of both the porous substrate and the membrane layer.

The preparation of LaWO asymmetric membranes for hydrogen separation brings many challenges concerning the shape and microstructure of the final assembly. The bending effects due to the different shrinkage rates of the LaWO gas-tight membrane and the porous LaWO substrate prevent the successful sealing of the membrane in the H_2-permeation test module, thus making further performance measurements impossible. Hence, a detailed understanding of the sintering behaviour of these two components is of great importance. Additionally, the microstructural adjustment of the membrane and substrate represents another key point in the preparation process. To the best of our knowledge, there are no studies on these complex manufacturing issues with respect to the LaWO material. Furthermore, we are not aware of any studies on the preparation of LaWO-supported LaWO membranes with optimised microstructure. The present paper aims to close this gap.

Table 1
Chemical compatibility of LaWO with SOFC state-of-the-art substrate components. The membrane material and substrate component were mixed in 1:1 weight ratio, and heat treated at temperatures between 600 °C and 1400 °C. The resulting products were investigated by XRD [47].

Membrane material	Substrate component	600 °C/12 h	800 °C/12 h	1100 °C/5 h	1400 °C/5 h
LaWO	CGO	No reaction	No reaction	No reaction	Solid solution
LaWO	NiO	No reaction	No reaction	La$(Ni_{0,8}W_{0,2})O_3$ $La_{1,83}NiO_{3,84}$ $La(NiO_3)$	La$(Ni_{0,8}W_{0,2})O_3$ $La_{1,83}NiO_{3,84}$ $La(NiO_3)$
LaWO	YSZ	No reaction	No reaction	$La_2Zr_2O_7$	$La_2Zr_2O_7$

2. Experimental section

2.1. Preparation of single layers and asymmetric membranes

In order to study the thermal behaviour of LaWO membranes and to learn more about layer densification, shrinkage and microstructural evolution, experiments were organised in two major stages. First, single membrane and single substrate layers were prepared independently; second, asymmetric membranes consisting of membrane–substrate assemblies were prepared. The starting ceramic powders and manufacturing approaches, as well as the characterisation techniques are described in the following section.

2.1.1. Initial ceramic powders

In the present study, ceramic powders with a stoichiometry of $La_{5.4}WO_{12-\delta}$ were used to prepare the membrane and substrate layers. The powders were synthesised by two approaches: spray pyrolysis (commercially available powder from CerPoTech, Norway) and solid state synthesis (powder produced in-house).

2.1.1.1. LaWO powder via the solid state reaction (SSR). The powder used for membrane preparation was synthesised via the solid state reaction (SSR). For this purpose, stoichiometric amounts of La_2O_3 (99.999%, Sigma Aldrich) and WO_3 (99.995%, Sigma Aldrich) were mixed and homogenised by means of ball milling in ethanol with 8YSZ milling balls. After drying, the powder mixture was thermally treated at 1500 °C for 12 h to accomplish the solid state reaction. The resulting powder was additionally milled in a planetary ball mill and sieved through a sieve with 32 μm mesh size. The mean particle size D_{50} was estimated as 0.8 μm and the specific surface area of the powder was 1.9 m²/g. A high purity of the powder was achieved with this synthesis method. This is essential for a good working membrane.

2.1.1.2. LaWO powder via the spray pyrolysis process (SP). The powder used for substrate preparation was the commercially available LaWO with a La/W ratio of 5.4 (CerPoTech, Norway) produced by spray pyrolysis (SP) and calcined at 600 °C [48]. For the substrate layers large amounts of the powder were needed. For this reason a commercial powder was chosen. Also small amounts of impurities could be accepted in the substrate, as long as they were not affecting the membrane layer. The chemical composition, particle size and specific surface area were analysed for the as-delivered powder. The chemical analysis revealed a La/W ratio of 5.4 and small amounts of impurities, consisting of Al (0.028 wt%) and Na (0.14 wt%). The particle size of the SP powder was D_{50}=0.8 μm and the specific surface area ($A_{spec.}$) was determined as about 7 m²/g.

In order to adjust the specific surface area and the respective sintering activity of the commercial LaWO powder, an additional thermal treatment and milling step were necessary prior to the preparation of slurry with optimal properties. This slurry was used subsequently in the tape-casting process. This is shown detailed in Section 3.1.

2.1.2. Preparation of the tape-casting slurry

For the tape casting of membrane and substrate layers, organic-based ceramic suspensions were produced separately. The necessary components are listed in Table 2. The used solvent was a mixture of Ethanol and MEK. The dispersing agent had the function to separate single particles in the solution. The binder and the plasticisers granted the mechanical stability and flexibility of the green tapes. The slurries used for membrane and substrate preparation (referred to as membrane slurry and substrate slurry, respectively), have two process steps in common: (i) mixing of the solvent, dispersing agent, ceramic powder, and milling media in a certain ratio to form the initial suspension, and (ii) addition of the binder and plasticiser. Each step was followed by homogenisation in a Thinky ARV310CE planetary mixer. As a specific step for the preparation of the substrate slurry, a pore forming agent was also added in 25 wt% of the solid load to the initial slurry, and the mixture was additionally homogenised. To completely dissolve the binder, the two slurries were left to rest for about 48 h before being used in the tape-casting experiments.

Table 2
Components used for the tape-casting slurry.

Slurry components	Chemicals for membrane slurry	Chemicals for substrate slurry
Ceramic powder	$La_{5.4}WO_{12-\delta}$ (SSR)	$La_{5.4}WO_{12-\delta}$ (SP)
Pore former	–	Rice starch
Solvent	Ethanol/MEK	Ethanol/MEK
Dispersing agent	Nuosperse FX 9086	Nuosperse FX 9086
Binder	PVB-98	PVB-98
Plasticiser type I	Solusolv S2075	Solusolv S2075
Plasticiser type II	PEG 400	PEG 400

2.1.3. Processing via tape casting

In the present work, the membrane and substrate single layers, as well as asymmetric structures/assemblies, consisting of a 20–30 μm-thick dense membrane layer supported by a 250–350 μm-thick porous substrate layer, were processed by sequential tape casting. The tape-casting experiments were carried out with the KAROcast 300-7 micro-tape-casting device from KMS Automation GmbH, Germany. Before the slurries were used in the tape-casting experiments, they were homogenised and de-aired by applying a vacuum within the mixing device.

The process consists of first casting the membrane layer onto the polymeric foil, which moves with controlled speed into the vented chamber of the instrument. The foil is composed of PET (Polyethylene terephthalate) and has a thickness of 100 μm. After the membrane layer has completely dried at ambient conditions, the substrate layer is cast on top of the membrane layer. This method enables the formation of defect-free functional membrane layers because of the high surface quality of the polymer foil (smooth and defect-free). This represents a major difference compared to conventional tape casting, where the substrate layer is first cast on the polymeric foil, and the membrane layer is then formed on top of the substrate surface. The latter has a reduced smoothness, and thus strongly affects the quality of the top membrane layer. For sintering and further investigations the tapes are removed from the carrier foil after the drying process. The complete procedure is shown schematically in Fig. 1.

In total, three types of tapes were cast: single substrate layers, single membrane layers, and membrane–substrate assemblies. The targeted thicknesses of the single substrate layers were the same as those of the membrane–substrate assemblies, namely 320 μm in the green state. However, the thickness of the single membrane layer (65 μm in the green state) is higher than that of the membrane layer in the assembly geometry (36 μm in the green state) due to issues related to the mechanical instability of such thin unsupported layers. The drying time depends on layer thickness and ranged between 3 h and 12 h. The airflow was kept constant (45 m³/h) during the entire drying processes. To achieve sufficient clarity in terms of the selected experimental conditions, including the manufacturing parameters, and the produced samples used for further characterisation, a summary is presented in Table 3.

For the nomenclature of dimensions and shrinkage directions the tape-casting direction is defined as the x-direction, the transverse direction is y and the thickness direction is represented by z. The tape-casting (x) and transverse (y) directions are called lateral directions. These correspond to the directions in which the tape/layer experiences shrinkage forces, as will be discussed later. When the tape/layer shrinks equally in all directions ($\varepsilon_x = \varepsilon_y = \varepsilon_z$), this is considered isotropic shrinkage behaviour. In reality, the shrinkage behaviour of tape-cast membrane and substrate layers deviates from the ideal isotropic case, as will be demonstrated in the case of the LaWO membrane and LaWO substrate layers, both as independent components and as an assembly.

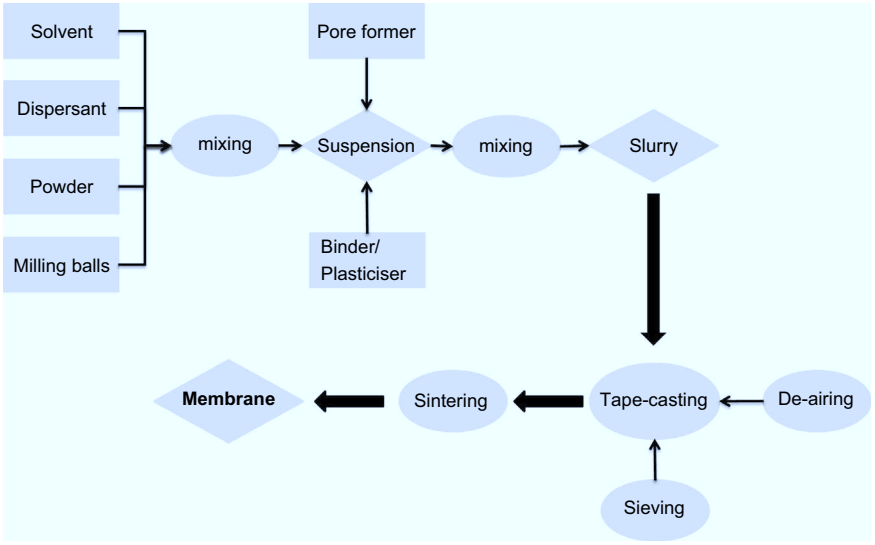

Fig. 1. Schematic of process steps for the fabrication of single membrane and substrate layers as well as of asymmetric membrane–substrate structures all based on LaWO.

Table 3
Summary of the tape-casting parameters used for fabrication of LaWO tapes of three different types: single membrane layer (M), single substrate layer (S), and asymmetric assembly (MSA) consisting of a membrane (MSA-M) and a substrate (MSA-S). In addition, the final thickness is given.

Reference name	Powder	Blade gap [μm]	Casting speed [mm/s]	Drying time [h]	Green thickness [μm]	Final thickness [μm]	Investigations
Single layer							
M	SSR	250	5	6	65	50	Shrinkage, microstructure
S	SP	800	2.5	12	320	210	Shrinkage, microstructure
Membrane–substrate assembly							
MSA-M	SSR	100	5	3	36	30	Bending, microstructure, He leakage
MSA-S	SP	800	2.5	12	320	200	
MSA	SSR/SP	–	–	15	356	230	

2.1.4. Samples for shrinkage measurements

The samples for shrinkage measurements were prepared from the dried tape by cutting off strips with a width of 15 mm and shaping them into cylinders. The shrinkage was studied using the optical dilatometer by measuring the dimensional change in the *z*-direction of the cylinder during sintering. For this purpose, the tapes were thermally treated at temperatures up to 1500 °C with a heating ramp of 5 °C/min and a dwell time of 3 h.

2.1.5. Samples for microstructural investigations

For microstructural analyses, disc samples with diameters of 22–26 mm were cut out from the three kinds of green tapes and sintered up to 1500 °C for 3 h. Sequential tape-cast samples with the same geometry were used to study the bending behaviour. For this purpose, they were sintered in the optical dilatometer.

2.2. Characterisation techniques

The particle size distribution (PSD) and specific surface area (BET [49]) of the starting powders used to prepare the single layers and asymmetric structures were carefully monitored and controlled. PSD measurements were carried out using a Horiba LA-950 V2 from Retsch Technology. BET measurements were performed using an Areameter from Ströhlein with Nitrogen as measurement gas at a temperature of −196 °C.

The thermal behaviour of the tape-cast LaWO layers was studied by performing systematic sintering experiments with a TOMMIplus optical dilatometer (Fraunhofer ISC, Würzburg, Germany). The sample with known dimensions was positioned on the sample holder within the instrument chamber, where it was gradually heated. Images of the sample silhouette were periodically recorded with a charge-coupled device (CCD) camera during heat treatment. To achieve high contrast, a monochromatic light source was mounted opposite the camera. For the measurements in this work, heating ramps of 1–5 °C/min and temperatures up to 1500 °C with dwell times up to 3 h were used. Pictures of the sample silhouette were taken every 60 s during heat treatment. The measurement software TOMMI online (Fraunhofer ISC, Würzburg, Germany) was used to analyse the corresponding shrinkage of the samples based on the recorded images.

A thermo-gravimetric analysis (TGA) was performed to investigate the decomposition behaviour of the organic additives in the tape-cast samples using a Netzsch STA 409C system. The heating rate was 3 °C/min with a maximum temperature of 1000 °C. The applied atmosphere was air at ambient pressure.

To investigate the microstructure of tape-cast samples, scanning electron microscopy (SEM) was performed using a Phenom electron microscope manufactured by FEI with a backscattered electron detector and acceleration voltage of 5 kV. For powder investigation, a Zeiss Ultra 55 electron microscope with an acceleration voltage of 15 kV and a backscattered detector was used.

The porosity, layer thickness, and pore size of the sample's cross section were quantified using image analysis with the AnalySIS pro software (Olympus Soft Imaging Solutions GmbH).

The shape and topography of the samples were monitored by means of a CT350 T device from Cyber Technologies using a confocal white light sensor. The *z*-resolution of the sensor was 0.1 μm and the spot size was 12 μm.

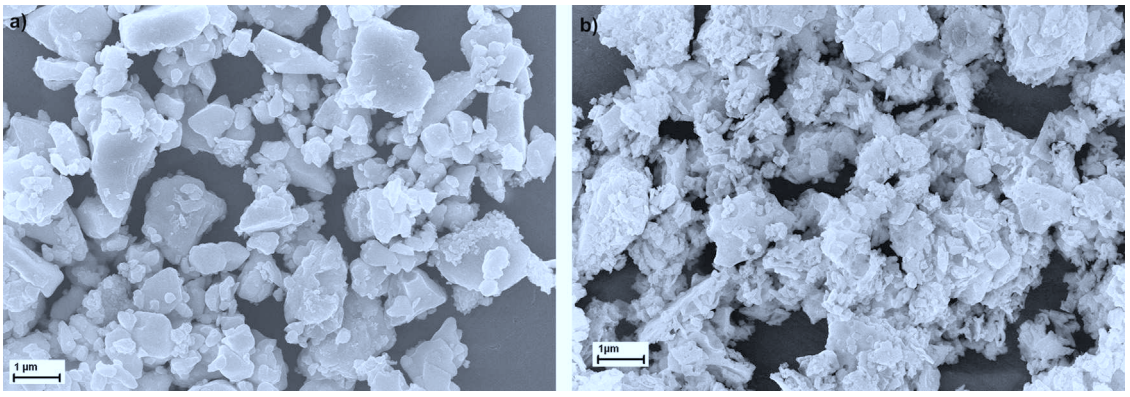

Fig. 2. SEM images showing (a) LaWO powder produced in-house after milling and (b) commercial LaWO powder from CerPoTech as calcined at 600 °C.

He leakage tests were performed on sintered asymmetric membranes by means of a Pfeiffer leakage test setup. For this purpose, the samples were sealed with a rubber sealing on the membrane side, and a pressure difference of 1000 hPa was applied. Afterwards, He was fed over the substrate side. Permeating He was analysed by a mass spectrometer. The measured area was always 1 cm² due to the geometry of the sample holder and the rubber sealing. The result is displayed in hPa dm³ cm^{-2} s^{-1}. A maximal value of $1 \cdot 10^{-3}$ hPa dm³ cm^{-2} s^{-1} was set as the threshold He leakage rate. Membranes displaying values higher than this were not accepted as gas-tight.

3. Results and discussion

3.1. Powder ccharacterisation

The LaWO powder produced in-house via the solid state reaction had a particle size of D_{50}=0.8 µm and a specific surface area A_{spec} of 1.9 m²/g after milling. The powder particles revealed uniform morphology (Fig. 2a).

The commercial LaWO powder produced by spray pyrolysis tended to form agglomerates very easily. The particle morphology was rather irregular and angled, which explains the high surface area (Fig. 2b). Due to the high surface area, the initial powder was not suitable for tape-casting. An additional heat treatment was thus required to adjust the sintering activity by reducing the powder surface area (as already explained in Section 2.1.1).

3.2. Pre-treatment of the spray pyrolysis powder

The shrinkage of a pressed sample of commercial LaWO powder synthesised via spray pyrolysis was measured in a preliminary experiment. Sintering of the powder began at around 1150 °C. At the end of heat treatment, the residual porosity of the specimen was less than 1%, which was determined optically by means of image analysis (Analysis Pro software).

For further experiments with layered structures, a pre-calcination temperature for the SP powder of 1200 °C was chosen to reduce sintering activity and to allow better adjustment of layer shrinkage. This temperature was slightly above the initial sintering temperature of 1150 °C for the sample. The calcined spray pyrolysis powder had a particle size of D_{50}=1.2 µm and a specific surface area of $A_{spec.}$=3.4 m²/g. Table 4 summarises the mean particle size (D_{50}) and specific surface area ($A_{spec.}$) of the powders that were used for membrane and substrate layer fabrication.

Table 4
Mean particle size (D_{50}) and specific surface area ($A_{spec.}$) of the powders used for membrane and substrate layer fabrication.

Powder/method	State	D_{50} (µm)	$A_{spec.}$ (m²/g)	Application
LaWO/SSR	As produced	0.8	1.9	Membrane
LaWO/SP	As delivered	0.8	7.0	–
LaWO/SP	Pre-treated	1.2	3.4	Substrate

3.3. Sintering studies of the tape-cast layers

Three different LaWO-based tapes were fabricated by means of tape casting for further investigations: single substrate layers (S), single membrane layers (M), and membrane–substrate assemblies (MSA), as shown in Table 3.

3.3.1. Green densities

The green densities of the tape-cast layers were determined by measuring the dimensions and weight of the samples. The membrane layers had a green density of 55% of the theoretical density. The density of the substrate layers was 20% due to the high amount of organic additives, including the pore former.

3.3.2. Optimisation of the de-binding process

To prepare a defect-free membrane, the organic components in the green membrane and substrate tapes must be released gradually to avoid damaging the resulting layer. With the aim of developing a suitable temperature programme for sintering the tape-cast layers, the release of organic components was investigated in a thermo-gravimetric study. For this, a substrate tape specimen was used because it contained a higher amount of organic components, which naturally leads to stronger mass changes during the thermo-gravimetric analysis. The resulting curve shown in Fig. 3 reveals that the largest mass loss (34%) was recorded in the temperature range from 200 °C to 400 °C, which is associated with a very intensive release of organic components. At higher temperatures, around 650 °C, the last organic residues were removed.

Based on this result, the tape-cast samples were heated with a heating rate of 1 °C/min up to 600 °C. Afterwards, heating rate was increased (5 °C/min) and sintering was performed at selected temperatures. This additional de-binding heat treatment step ensures the complete and homogenous release of the organic components from the tape.

3.3.3. Single layers

The sintering behaviour of the single membrane and substrate layers was investigated by optical dilatometry. Details on sample

preparation and the geometry used in this section, as well as the method, have already been given in the experimental section.

The height reduction of the cylinders was considered to be a good approximation of the free shrinkage of the tape, as reported in [50] for CGO tapes. No deviation of the shrinkage between the transverse *y*-direction and the casting *x*-direction was detected.

Fig. 4 displays the change in cylinder height as a function of time and temperature based on optical dilatometry. By analysing the recorded curves, four zones can be distinguished (denoted as I, II, III and IV), which represent different stages of the sintering process. The red curve designates the single membrane layer, while the black one stands for the single substrate layer.

For the single membrane layer (M-tape), only one shrinkage step could be ascertained, illustrated by zone III. The sintering of the membrane layer started at about 1250 °C (beginning of zone III), and full densification, where no further shrinkage occurred, was achieved after 50 min at 1500 °C (beginning of zone IV). There was practically no difference in the sintering behaviour between the two layers in the low-temperature zones I and II.

As expected, the single substrate layer (S-tape) exhibited very different behaviour. About 30 min after the sintering programme began (Fig. 4, zone I), 3% shrinkage was recorded. The reason for this initial shrinkage is related to the release of the organic components from the green tape. Substrate sintering started at about 1300 °C (zone III). After the most significant part of the densification processes was accomplished at about 1500 °C, the substrate shrank continuously with the dwell time at 1500 °C (zone IV). This can be explained by the residual porosity of the substrate, which is, however, of an essential importance for the proper functioning of the substrate.

Due to the continuous shrinkage of the substrate layer compared to the membrane layer, we assumed a mismatch in the thermal behaviour of the two single layers. Such different behaviour would lead to curvature when the two components are assembled and co-fired, and represents an important manufacturing issue requiring further optimisation.

The total shrinkage of the substrate layer (black curve) in the full temperature and time window was about 36% after 3 h at 1500 °C. This value was almost twice as high as that of the membrane layer (17% after 3 h at 1500 °C, red curve). This was caused by the different green densities of the layers and the different amounts of organic components contained within them. In the case of the membrane layer, the green density was 55%, while for the substrate, it was 20%.

The corresponding strain rates for the two single layers are shown in Fig. 5. Similar to the previous figure, four zones can be distinguished, denoting the different sintering stages. The substrate layer (black curve) exhibited a higher sintering rate than the membrane layer. The maximal strain rate for the substrate was reached after 285 min at a temperature of about 1450 °C. Analogically, the maximal sintering rate for the membrane layer (red curve) was reached at a similar temperature of about 1420 °C. It was observed that the sintering rates of the two layers decreased in the isothermal region (at 1500 °C, end of zone III).

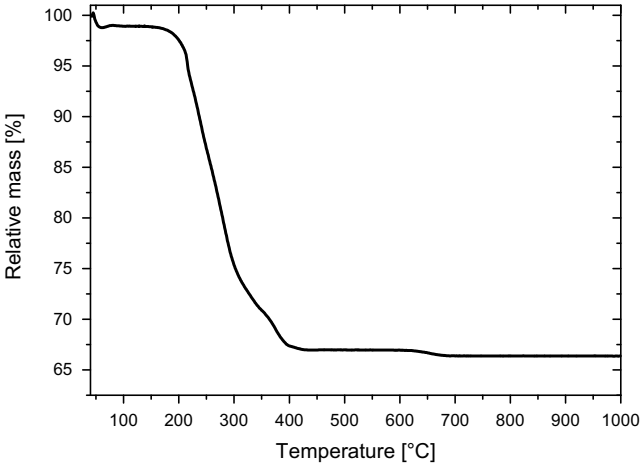

Fig. 3. Thermo-gravimetric curve of the tape-cast LaWO substrate.

3.3.4. Membrane–substrate assemblies (MSA-tape)

The co-firing of the asymmetric membrane–substrate assembly led to the constrained sintering of the two layers, which is a rather complex process. The mismatch of the sintering rates, which is represented by the difference between the individual sintering rates of the membrane and substrate layer (shown in Fig. 6), indicated that substrate shrinkage dominates over membrane shrinkage during thermal treatment. Practically, these effects

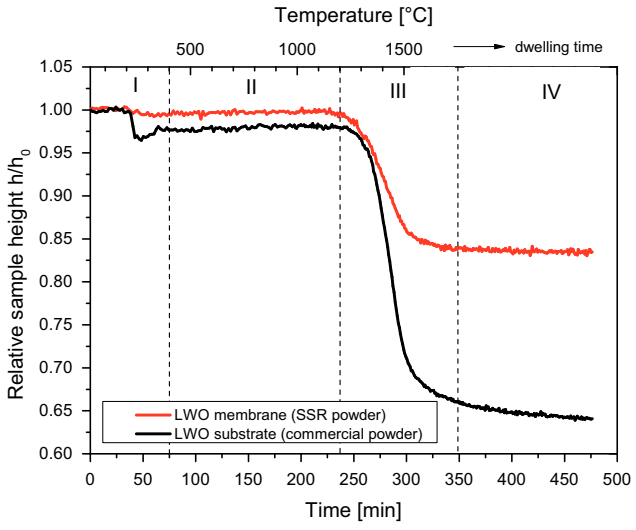

Fig. 4. Shrinkage of LaWO cylinders prepared from membrane and substrate single layers by tape casting. (For interpretation of the references to colour in this figure, the reader is referred to the web version of this article.)

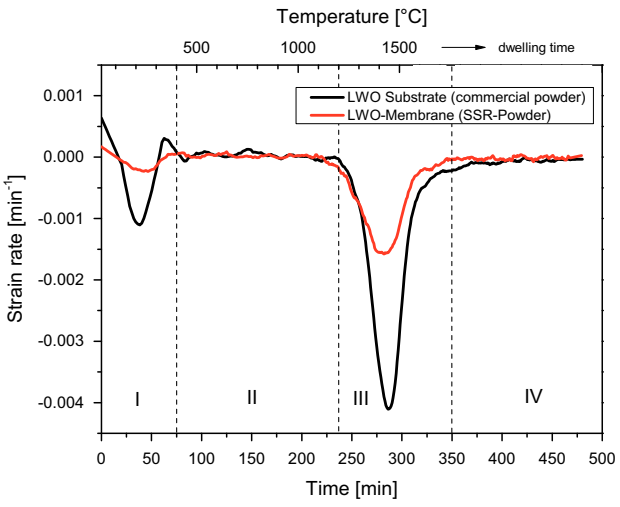

Fig. 5. Strain rates of the tape-cast LaWO membrane and substrate layers. (For interpretation of the references to colour in this figure, the reader is referred to the web version of this article.)

result in bending of the membrane–substrate assembly in the substrate direction, as mentioned above. In this context, the dependency of the curvature of bi-layers on the mismatch of the sintering rates of single layers was reported in [51,52], and is expressed by Eq. (2):

$$\dot{k} = \frac{6(m+1)^2 mn}{m^4 n^2 + 2mn(2m^2+3m+2)+1} \Delta\dot{\varepsilon} \quad (2)$$

where $\dot{k}$ is the normalised degree of curvature; m is the ratio of layer thicknesses; n is the ratio of viscosities and viscous Poisson ratios of the layers; and $\Delta\dot{\varepsilon}$ is the mismatch of sintering rates of the two layers.

Thus, the larger mismatch in strain rates between the layers potentially leads to greater curvature of the bi-layer assembly.

In order to investigate the bending phenomena in more detail, a thermal study and analysis were carried out on a membrane–substrate system prepared by sequential tape casting (for tape properties, see Section 2.1.3).

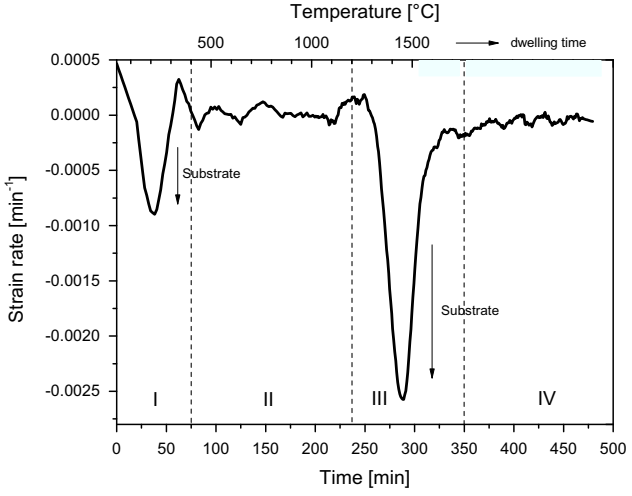

Fig. 6. Mismatch of strain rates (difference between individual strain rates of membrane and substrate layer) between LaWO membrane and substrate single layers determined as the net difference between the red and black curves in Fig. 5.

Fig. 7 shows a series of images recorded by the optical dilatometer during the heat treatment of the asymmetric assembly. The two-layered tape was placed on the underlying plate of MgO with the membrane side facing up.

As the sintering began at 1200 °C, a slight bending in the membrane direction was recorded (Fig. 7a). This may have been caused by the earlier sintering of the membrane compared to the substrate layer (see Fig. 4). As the temperature increased, the observed bending was compensated by the substrate, and the sample became flat at 1300 °C (Fig. 7b). At higher temperatures, the substrate gradually became the dominating source of shrinkage with higher strain rates than the membrane layer. This effect caused strong bending towards the substrate at 1500 °C (Fig. 7c) and it was particularly pronounced at the edges of the disc sample. Nevertheless, the middle part of this asymmetric assembly remained flat, no spherical shape was developed. Fig. 8 illustrates the curvature recorded by white light topography of the LaWO membrane–substrate assembly after sintering at 1500 °C.

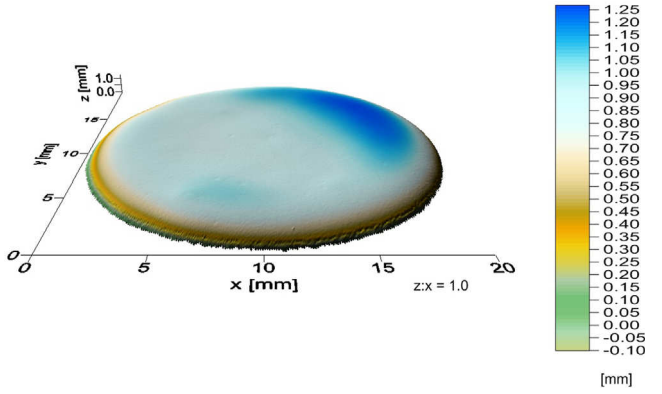

Fig. 8. White-light topography image of an asymmetric LaWO membrane after sintering at 1500 °C illustrating the obvious edge bending (in yellow) and the middle flat area. (For interpretation of the references to colour in this figure legend, the reader is referred to the web version of this article.)

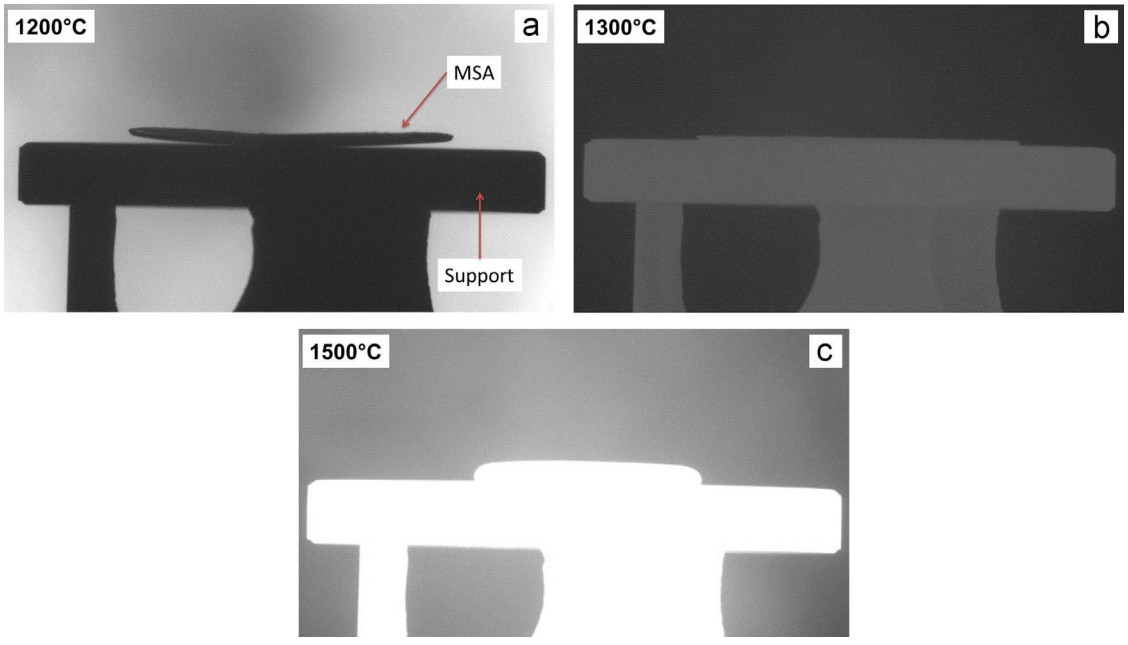

Fig. 7. Images of the asymmetric LaWO system taken with the optical dilatometer. The analysed specimen consisted of an asymmetric membrane–substrate assembly with the membrane layer facing up.

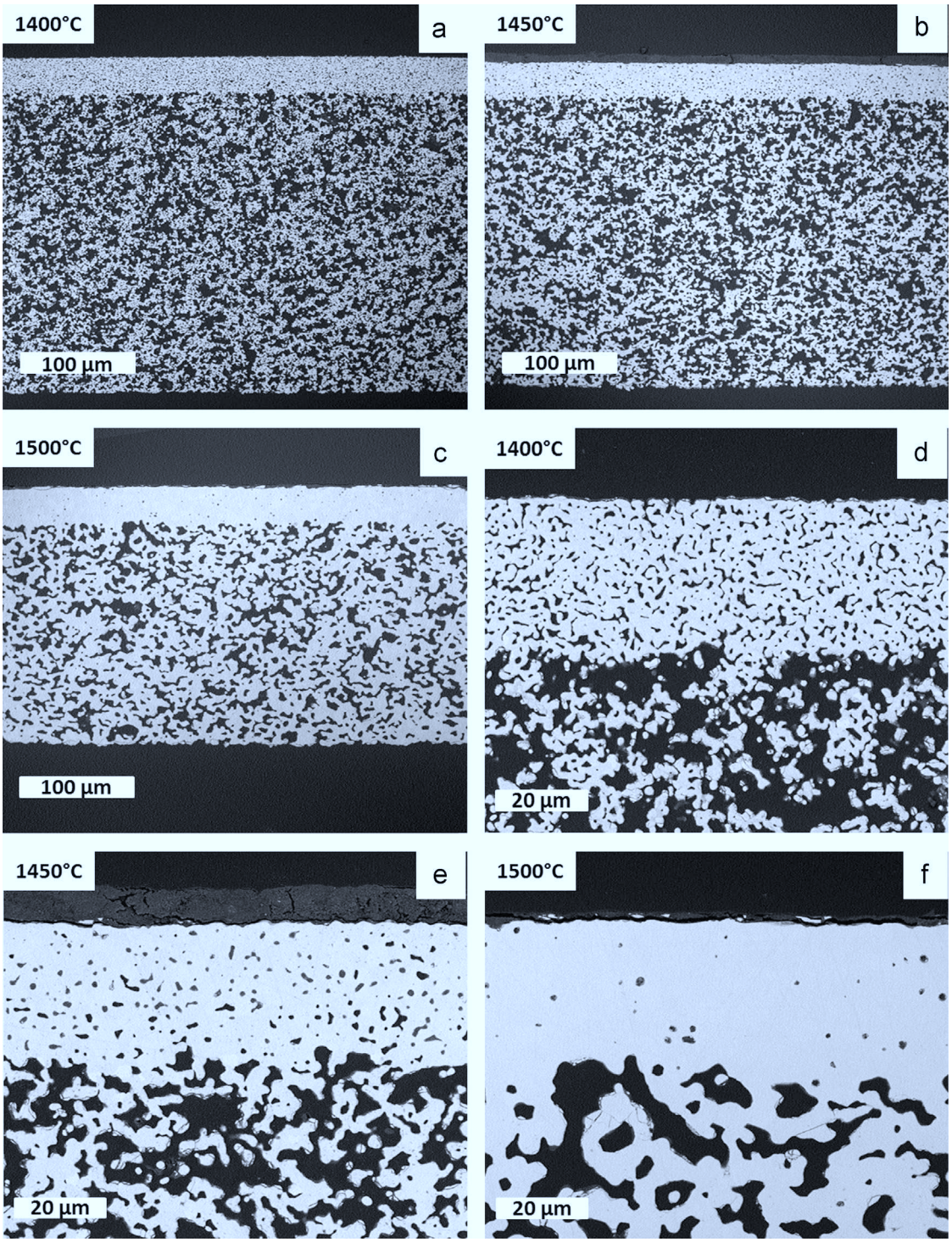

Fig. 9. SEM micrographs of sintered asymmetric LaWO membrane systems at different temperatures and equal magnification (a)+(d) 1400 °C; (b)+(e) 1450 °C; (c)+(f) 1500 °C.

3.4. Microstructure

In order to observe the microstructural evolution with temperature and thus better understand the sintering process of LaWO-based asymmetric membrane assemblies, a detailed microstructural analysis was performed.

Fig. 9 displays SEM images showing the microstructure of a tape-cast asymmetric LaWO membrane at different sintering temperatures. Images (a)–(c) are an overview of the complete asymmetric assembly. Images (d)–(f) were taken at higher magnification near the membrane–substrate interface with a complete view of the membrane layer.

3.4.1. Membrane layer in MSA (MSA-M)

As the images clearly illustrate, the selected temperature range (1400–1500 °C) was most important for the development of the required combination of microstructures as the largest shrinkage

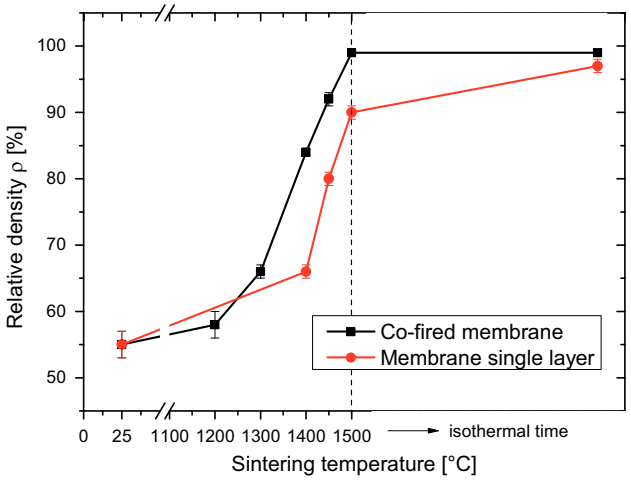

Fig. 10. Density evolution of LaWO membrane single layers and co-fired membrane–substrate assemblies versus the sintering temperature and isothermal dwell time.

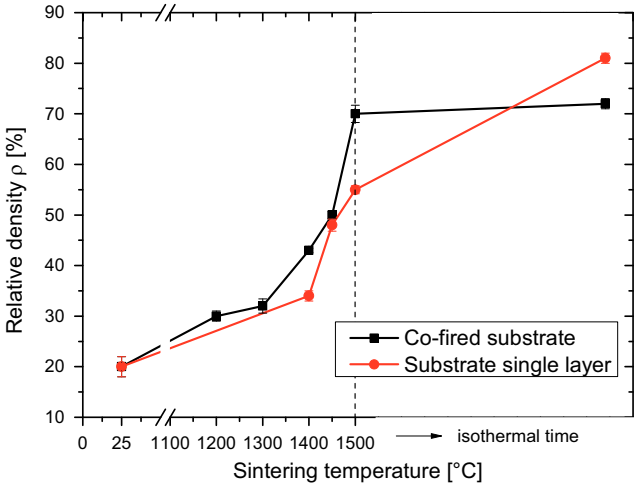

Fig. 11. Density evolution for the LaWO substrate layers co-fired with a membrate and also sintered as a single layer.

and full densification of the LaWO membrane occur here. As shown in Fig. 9c, only isolated pores exist and there are no continuous pore channels visible in the membrane, as is the case for lower sintering temperatures (Fig. 9a and b). For the optimal operation of a H_2 separation membrane, a residual closed porosity of less than 5% is needed to ensure the required gas-tightness.

With the aid of the SEM microscopic analysis, and more particularly, of the image analysis by means of the specialised software, the densification of the asymmetric LaWO membranes during heat treatment was investigated further.

Fig. 10 shows the relative density as a function of the sintering temperature and isothermal dwelling time for both the single membrane layer and membrane–substrate assembly.

As can be seen from Fig. 14, the two membrane layers (single membrane and membrane layer in the assembly) have the same starting porosity because of the identical slurry compositions. The final density of the single membrane layer was determined as about 97% at 1500 °C after 3 h. The membrane layer co-fired in assembly with the porous substrate exhibited a relative density of 99% at the same conditions. This higher densification resulted from the simultaneously shrinking substrate. Furthermore, in the co-fired layer assembly, densification occurred at temperatures around 100 °C lower than in the single membrane layer, as shown in Fig. 10.

3.4.2. *Substrate layer in MSA (MSA-S)*

A similar image analysis was performed for the substrate layers. The density evolution of a co-fired and a single substrate layer is shown in Fig. 11. Both layers (single substrate layer and substrate layer in the assembly) initially revealed a relative density of 20%. The co-fired layer showed a considerable increase in density from 43% to 70% between 1400 °C and 1500 °C. The density of the single layer increased from 34% to only 55% in the same temperature range. During isothermal dwell treatment, the single substrate layer reached a density of 81%, while the density of the substrate layer co-fired in assembly was 72%. Hence, a density difference of about 9 percentage points can be ascertained for the two layers in the final sintering stage. The value of 19% porosity for the single substrate is too low for an efficient gas supply to the membrane.

The analysis of the densification process of the tape-cast LaWO asymmetric membranes allows us to conclude that the maximal sintering temperature of the co-fired LaWO layers is lower than 1500 °C and the isothermal dwell time should be adjusted very

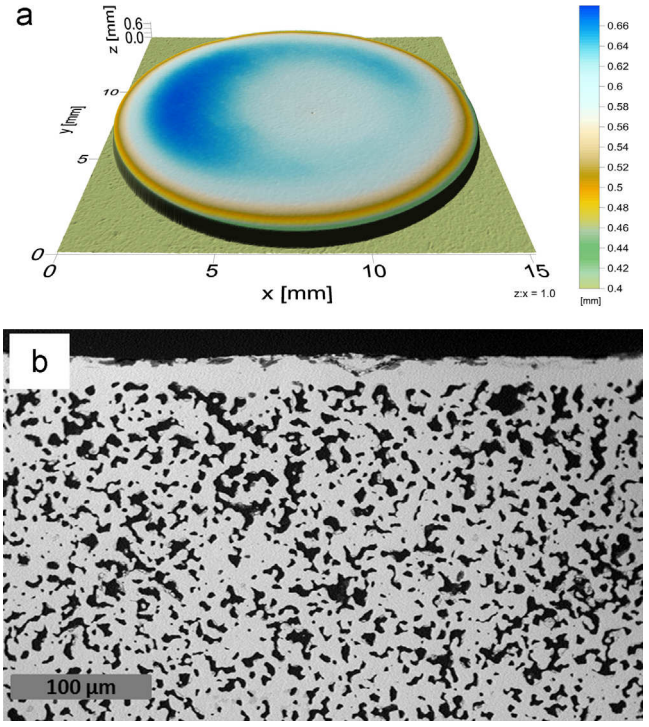

Fig. 12. (a) Topography image and (b) SEM micrograph of an optimised LaWO membrane–substrate assembly in disc geometry sintering conditions: 1450 °C for 6 h.

carefully to achieve an optimal microstructure both for the membrane and the substrate.

An optimised temperature programme was therefore additionally developed with a maximal temperature of 1450 °C and a dwell time of 6 h. It led to gas-tight membrane layers with a relative density of 97% and a He leakage of 10^{-5} hPa dm³ cm^{-2} s^{-1}. This value is comparable to other He leakages achieved for SOFC-electrolytes [40] and oxygen transport membranes [42]. Under these sintering conditions, the substrate porosity was retained at about 30%, which approaches the required value for practical application (30–40%). The bending could be then reduced to a total height difference of only 40 µm, which can be seen in the topography image in Fig. 12a and the SEM image of the MSA microstructure in Fig. 12b.

3.5. Effect of the fabrication process and the shrinkage forces during sintering on the MSA microstructure and geometry

This section focuses on the influence of the manufacturing technique on the MSA microstructure and its evolution during heat treatment.

During the tape-casting process, the slurry consisting of ceramic particles dispersed in a liquid phase is exposed to shearing forces, ultimately leading to a certain particle orientation and later to anisotropic shrinkage.

For the thick substrate layer, shearing under the doctor blade must have been lower than for the much thinner membrane layer, reducing preferential particle orientation. This effect was also shown by Raj et al. in [53], where the anisotropy in the tape-cast layers was investigated in dependence on the layer thickness and casting velocity. They showed that anisotropy in the layers decreases with greater tape thickness and lower casting speed.

3.5.1. Membrane layer in MSA (MSA-M)

Fig. 13 presents membrane shrinkage in *z*-direction versus density for a single membrane and a co-fired membrane layer.

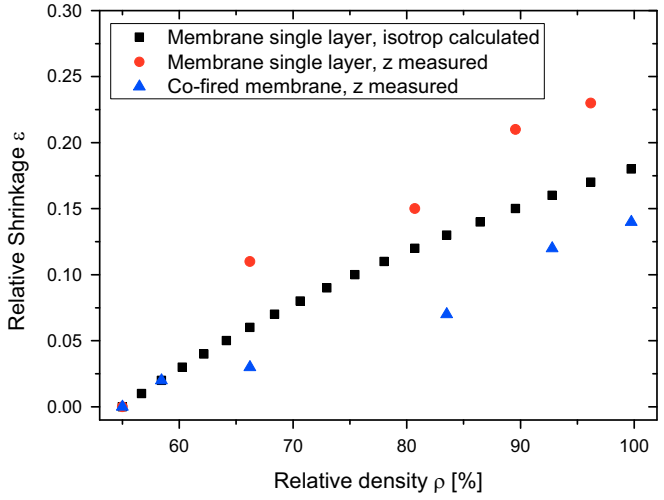

Fig. 13. Relative shrinkage as a function of the relative density displaying deviation from the isotropic behaviour of the membrane layers measured in the thickness direction *z*.

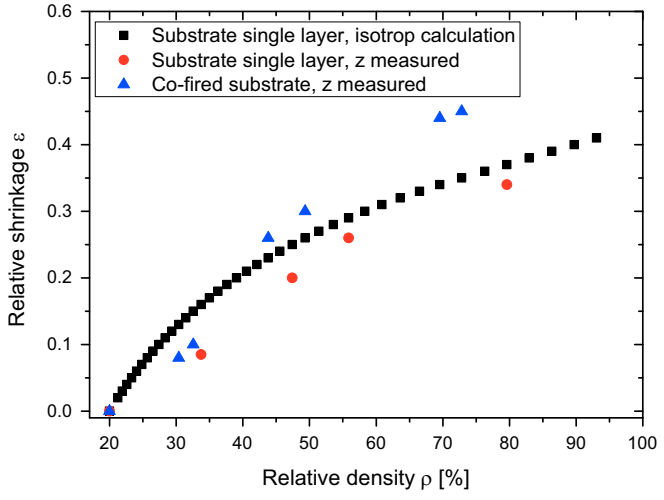

Fig. 14. Relative shrinkage as a function of the relative density displaying deviation from the isotropic behaviour of substrate layers measured in the thickness direction *z*.

The shrinkage was determined by image analysis. To show the deviation of the shrinkage from an optimal isotropic case, the isotropic shrinkage was calculated and added to Fig. 13. For the calculation, the following formula from [54] was used:

$$\rho = \frac{\rho_0}{\frac{\hat{E}}{(1-\varepsilon)}} \tag{3}$$

where ρ is the relative density, ρ_0 is the starting density, and ε is the isotropic shrinkage.

As can be seen from the figure, the shrinkage of the membranes (single membrane layer (in red) and membrane layer co-fired in assembly (in blue)) displays significant deviation from the calculated isotropic case (in black).

The greater shrinkage in the *z*-direction exhibited by the single layer can be explained by certain particle orientation due to the tape-casting technique, as discussed above, which led to the observed anisotropic shrinkage of the layer.

For the co-fired membrane layer, the opposite effect is visible. Shrinkage in the *z*-direction was lower than the calculated isotropic shrinkage. This observation is associated with the contact between the substrate and membrane layer, which also experiences shrinkage during the sintering process. To counteract membrane shrinkage, the substrate layer enhances lateral shrinkage thus leading to less shrinkage in the *z*-direction of the membrane.

3.5.2. Substrate layer in MSA (MSA-S)

Fig. 14 presents a similar dependence for the substrate layers. On the one hand, shrinkage of the single substrate layer corresponds quite well to the calculated behaviour, especially in the late sintering stage (relative density around 55%), resulting from the higher layer thickness and the lesser particle orientation, as highlighted above.

On the other hand, the behaviour of the co-fired substrate is more complicated. At the early sintering stage (relative density around 30%), substrate shrinkage is rather similar to that of the single layer: shrinkage in the *z*-direction is slightly lower than in the calculated isotropic case. At a relative density of about 40%, a change was observed resulting from the decreased shrinkage rate of the membrane layer. Since the thickness ratio between the substrate and the membrane is around 10, we can assume that the membrane layer slightly hindered lateral shrinkage of the substrate layer. This effect becomes more pronounced as heat treatment proceeds. This situation is illustrated schematically in Fig. 15.

When the membrane layer reaches high density thus becoming more rigid, it offers more and more resistance to the substrate layer. This causes stresses which hinder lateral shrinkage (*x*- and *y*-directions) within the substrate layer. Hence, densification of the substrate in the *z*-direction is preferential. The stress can therefore be compensated by deformation (bending) of the assembly. In any case, the gravitational force also has a pronounced effect, counteracting the bending, since the assembly is oriented with the membrane side up during sintering.

4. Conclusions

LaWO is a very intriguing candidate for a number of high-temperature H_2 separation processes due to its mixed proton–electron conductivity and high chemical and thermal stability. There have been very few attempts to develop supported LaWO-based membranes of reduced thickness in the range of 10–30 μm so far. Combining a gas-tight LaWO membrane layer with a porous supporting LaWO layer leads to a variety of fabrication issues, such as undesired bending effects.

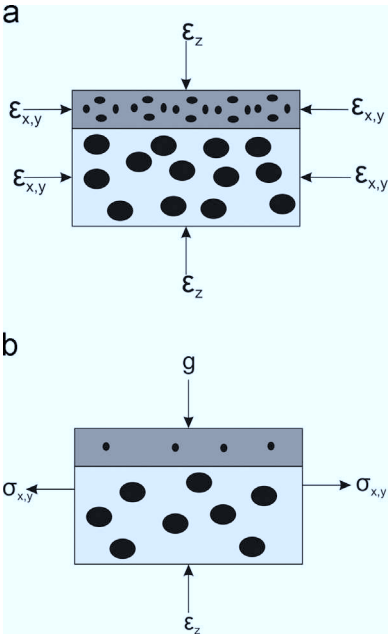

Fig. 15. Schematic of the densification of asymmetric membrane assemblies. The shrinkage forces and corresponding directions during sintering are denoted by arrows.

Single LaWO membrane and single LaWO substrate layers were prepared independently using the sequential tape-casting technology. The layer thickness was 65 μm for the membrane and 320 μm for the substrate layers in the green state. The same fabrication method was applied to prepare LaWO membrane–substrate assemblies with a total thickness in the green state of 370 μm.

The sintering behaviour of the single membrane and substrate layers was investigated intensively. The single substrate layer exhibited continuous shrinkage at 1500 °C with dwell time. This was due to the residual porosity of the substrate (19% of final porosity). The mismatch between the sintering rates for the membrane and substrate layers revealed that substrate shrinkage during thermal treatment of the membrane–substrate assembly dominated over membrane shrinkage, thus leading to undesired bending of the assembly. At the same time, thanks to the simultaneously shrinking substrate layer, a higher density (99%) was obtained for the co-fired membrane layer than for the single membrane layer (97%) at 1500 °C after 3 h. These results indicated that the temperature range of 1400 °C to <1500 °C is optimal for developing the required combination of membrane–substrate microstructures.

As was experimentally shown, the single membrane layer experienced greater shrinkage in the *z*-direction than the calculated isotropic case predicts. This is caused by certain particle orientation as an outcome of the tape-casting process. For the membrane layer in assembly, the opposite effect was found due to the counteracting substrate, which enhanced lateral (*x*-, *y*-) membrane shrinkage.

The series of thermal treatments and subsequent data analysis resulted in an optimised sintering programme (1450 °C/6 h). The resulting asymmetric LaWO membranes exhibited reduced bending (40 μm) and optimal density of the membrane layer (2–3% porosity) combined with optimal porosity (~30%) of the substrate layer. The LaWO membrane–substrate assembly displayed a He leakage in the order of 10^{-5} hPa dm³ cm^{-2} s^{-1}. The obtained optimised microstructure and reproducible architecture bring the LaWO supported structures a step forward towards upscaling and integration as system components in a variety of H_2-related applications.

Acknowledgements

This work was conducted thanks to the financial support granted within the Initiative and Networking Fund by the Helmholtz Association under the Portfolio MEM–BRAIN. Many thanks to Dr. D. Sebold for SEM imaging of the powders and to Mr. Kai Wilkner for conducting the white light topography. We would also like to acknowledge our colleagues at ZEA-3 for performing the ICP-OES analysis.

References

[1] A. Léon (Ed.), Hydrogen Technology – Mobile and Portable Applications, Springer-Verlag, Berlin Heidelberg, 2008.
[2] T. Norby, Solid-state protonic conductors: principles, properties, progress and prospects, Solid State Ion. 125 (1999) 1–11.
[3] J. Kniep, M. Anderson, Y.S. Lin, Autothermal reforming of methane in a proton-conducting ceramic membrane reactor, Ind. Eng. Chem. Res. 50 (2011) 12426–12432.
[4] H. Iwahara, T. Esaka, H. Uchida, N. Maeda, Proton conduction in sintered oxides and its application to steam electrolysis for hydrogen production, Solid State Ion. 3/4 (1981) 359–363.
[5] T. Norby, P. Kofstad, Electrical conductivity and defect structure of Y_2O_3 as a function of water vapor pressure, J. Am. Ceram. Soc. 67 (12) (1984) 786–792.
[6] K.-D. Kreuer, Aspects of the formation and mobility of protonic charge carriers and the stability of perovskite-type oxides, Solid State Ion. 125 (1999) 285–302.
[7] H.G. Bohn, T. Schober, Electrical conductivity of the high-temperature proton conductor $BaZr_{0.9}Y_{0.1}O_{2.95}$, J. Am. Ceram. Soc. 83 (2000) 768–772.
[8] H. Iwahara, H. Uchida, K. Ono, K. Ogaki, Proton conduction in sintered oxides based on $BaCeO_3$, J. Electrochem. Soc. 135 (1988) 529–533.
[9] R. Haugsrud, Y. Larring, T. Norby, Proton conductivity of Ca-doped Tb_2O_3, Solid State Ion. 176 (2005) 2957–2961.
[10] T. Shimura, M. Komori, H. Iwahara, Ionic conduction in pyrochlore-type oxides containing rare earth elements at high temperature, Solid State Ion. 86–88 (1996) 685–689.
[11] R. Haugsrud, T. Norby, Proton conduction in rare-earth ortho-niobates and ortho-tantalates, Nat. Mater. 5 (2006) 193–196.
[12] M.E. Ivanova, S. Ricote, W.A. Meulenberg, R. Haugsrud, M. Ziegner, Effects of A- and B-site (co-)acceptor doping on the structure and proton conductivity of $LaNbO_4$, Solid State Ion. 213 (2012) 45–52.
[13] M.E. Ivanova, W. Meulenberg, J. Palisaitis, D. Sebold, C. Solis, M. Ziegner, J. Serra, J. Mayer, M. Hänsel and O. Guillon, "Functional properties of $La_{0.99}X_{0.01}Nb_{0.99}Al_{0.01}O_{4-\delta}$ and $La_{0.99}X_{0.01}Nb_{0.99}Ti_{0.01}O_{4-\delta}$ proton conductors where X is an alkaline earth cation," J. Eur. Ceram. Soc., 2014.
[14] Mundschau Sammells (Ed.), Nonporous Inorganic Membranes, Wiley-VCH, Weinheim, 2006.
[15] T. Shimura, S. Fujimoto, H. Iwahara, Proton conduction in non-perovskite-type oxides at elevated temperatures, Solid State Ion. 143 (2001) 117–123.
[16] R. Haugsrud, Defects and transport properties in Ln_6WO_{12} (Ln=La, Nd, Gd, Er), Solid State Ion. 178 (2007) 555–560.
[17] J. Seeger, M.E. Ivanova, W.A. Meulenberg, D. Sebold, D. Stöver, T. Scherb, G. Schumacher, S. Escolástico, C. Solís, J.M. Serra, Synthesis and characterization of nonsubstituted and substituted proton-conducting $La_{6-x}WO_{12-y}$, Inorg. Chem. 52 (2013) 10375–10386.
[18] S. Escolástico, C. Solís, J.M. Serra, Hydrogen separation and stability study of ceramic membranes based on the system Nd_5LnWO_{12}, Int. J. Hydrog. Energy 36 (2011) 11946–11954.
[19] S. Escolástico, C. Solís, J.M. Serra, Study of hydrogen permeation in $(La_{5/6}Nd_{1/6})_{5.5}WO_{12-\delta}$ membranes, Solid State Ion. 216 (2012) 31–35.
[20] W. Meulenberg, M. Ivanova, H. Buchkremer, D. Stöver, J.S. Alfaro, S. Escolástico, CO2-tolerant, mixed conductive oxide and use thereof for hydrogen separation. International Patent WO 2012/010386 A1, 26 January 2012.
[21] R. Haugsrud, H. Fjeld, K.R. Haug, T. Norby, Mixed ionic and electronic conductivity of undoped and acceptor-doped Er_6WO_{12}, J. Electrochem. Soc. 154 (2007) B77–B81.
[22] S. Escolastico, V.B. Vert, J.M. Serra, Preparation and characterization of nanocrystalline mixed proton-electronic conducting materials based on the system Ln_6WO_{12}, Chem. Mater. 21 (2009) 3079–3089.
[23] C. Solís, S. Escolastico, R. Haugsrud, J.M. Serra, $La_{5.5}WO_{12-\delta}$ characterization of transport properties under oxidizing conditions: a conductivity relaxation study, J. Phys. Chem. C 115 (2011) 11124–11131.
[24] R. Haugsrud, C. Kjølseth, Effects of protons and acceptor substitution on the electrical conductivity of La_6WO_{12}, J. Phys. Chem. Solids 69 (2008) 1758–1765.
[25] A. Magraso, C. Frontera, D. Marrero-Lopez, P. Nunez, New crystal structure and characterization of lanthanum tungstate La_6WO_{12} prepared by freeze–drying synthesis, Dalton Trans. (2009) 10273–10283.
[26] M.E. Ivanova, J. Seeger, J.M. Serra, C. Solis, W.A. Meulenberg, W. Fischer, S. Roitsch, H.P. Buchkremer, Influence of the $La_6W_2O_{15}$ phase on the properties and integrity of $La_{6-x}WO_{12-\delta}$-based membranes, Chem. Mater. Res. 2 (2012) 56–81.

[27] A. Magrasó, J.M. Polfus, C. Frontera, J. Canales-Vázquez, L.-E. Kalland, C.H. Hervoches, S. Erdal, R. Hancke, M.S. Islam, T. Norby, R. Haugsrud, Complete structural model for lanthanum tungstate: a chemically stable high temperature proton conductor by means of intrinsic defects, J. Mater. Chem. 22 (2012) 1762–1764.
[28] S. Erdal, L.-E. Kalland, R. Hancke, J. Polfus, R. Haugsrud, T. Norby, A. Magraso, Defect structure and its nomenclature for mixed conducting lanthanum tungstates $La_{28-x}W_{4+x}O_{54+3x/2}$, Int. J. Hydrog. Energy 37 (2012) 8051–8055.
[29] S. Escolastico, J. Seeger, S. Roitsch, M. Ivanova, W.A. Meulenberg, J.M. Serra, Enhanced H2 separation through mixed proton–electron conducting membranes based on $La_{5.5}W_{0.8}M_{0.2}O_{11.25-d}$, ChemSusChem 6 (2013) 1523–1532.
[30] S. Escolástico, C. Solís, T. Scherb, G. Schumacher, J.M. Serra, Hydrogen separation in $La_{5.5}WO_{11.25-\delta}$ membranes, J. Membr. Sci. 444 (2013) 276–284.
[31] J. Roa, A. Magrasó, M. Morales, P. Núnez, M. Segarra, Determination of hardness, Young's modulus and fracture toughness of lanthanum tungstates as novel proton conductors, Ceram. Int. 37 (2011) 1593–1599.
[32] R. Vassen, X. Cao, F. Tietz, D. Basu, D. Stöver, Zirconates as new materials for thermal barrier coatings, J. Am. Ceram. Soc. 83 (2000) 2023–2028.
[33] V. Gil, J. Gurauskis, C. Kjølseth, K. Wiik, M.-A. Einarsrud, Hydrogen permeation in asymmetric $La_{28-x}W_{4+x}O_{54+3x/2}$ membranes, Int. J. Hydrog. Energy 38 (2013) 3087–3091.
[34] S. Baumann, W. Meulenberg, H. Buchkremer, Manufacturing strategies for asymmetric ceramic membranes for efficient separation of oxygen from air, J. Eur. Ceram. Soc. 33 (2013) 1251–1261.
[35] V. Gil, J. Gurauskis, M.-A. Einarsrud, Asymmetric supported dense lanthanum tungstate membranes, J. Eur. Ceram. Soc. 34 (2014) 3783–3790.
[36] S. Cheng, V.K. Gupta, J.Y. Lin, Synthesis and hydrogen permeation properties of asymmetric proton-conducting ceramic membranes, Solid State Ion. 176 (2005) 2653–2662.
[37] E. Vøllestad, C.K. Vigen, A. Magrasó, R. Haugsrud, Hydrogen permeation characteristics of $La_{27}Mo_{1.5}W_{3.5}O_{55.5}$, J. Membr. Sci. 461 (2014) 81–88.
[38] M. Weirich, J. Gurauskis, V. Gil, K. Wiik, M.-A. Einarsrud, Preparation of lanthanum tungstate membranes by tape casting technique, Int. J. Hydrog. Energy 37 (2012) 8056–8061.
[39] W. Schafbauer, F. Schulze-Küppers, S. Baumann, W. Meulenberg, N. Menzler, H. Buchkremer, D. Stöver, Tape casting as a multi purpose shaping technology for different applications in energy issues, Mater. Sci. Forum 706–709 (2012) 1035–1040.
[40] N.H. Menzler, J. Malzbender, P. Schoderböck, R. Kauert, H.P. Buchkremer, Sequential tape casting of anode-supported solid oxide fuel cells, Fuel Cells 14 (2013) 96–106.
[41] F. Schulze-Küppers, S. Baumann, W.A. Meulenberg, D. Stöver, H.-P. Buchkremer, Manufacturing and performance of advanced supported $Ba_{0.5}Sr_{0.5}Co_{0.8}Fe_{0.2}O_{3-d}$ (BSCF) oxygen transport membranes, J. Membr. Sci. 433 (2013) 121–125.
[42] S. Baumann, J. Serra, M. Lobera, S. Escolástico, F. Schulze-Küppers, W. Meulenberg, Ultrahigh oxygen permeation flux through supported $Ba_{0.5}Sr_{0.5}Co_{0.8}Fe_{0.2}O_{3-d}$ membranes, J. Membr. Sci. 377 (2011) 198–205.
[43] G.N. Howatt, R.G. Breckenridge, J.M. Brownlow, Fabrication of thin ceramic sheets for capacitors, J. Am. Ceram. Soc.30 (1947) 237–242.
[44] Q. Zhang, X. Luo, W. Li, H. Zhuang, D. Yan, Tape casting of AlN/glass composites for LTCC substrate, J. Mater. Sci. 38 (2003) 1781–1785.
[45] L. Palmqvist, K. Lindqvist, C. Shaw, Porous multilayer PZT materials made by aqueous tape casting, Key Eng. Mater. 333 (2007) 215–218.
[46] R.E. Mistler, E.R. Twiname, Tape casting, The American Ceramic Society, 2000.
[47] J. Seeger, Entwicklung protonenleitender Werkstoffe und Membranen auf Basis von Lanthan-Wolframat für die Wasserstoffabtrennung aus Gasgemischen (Dissertation), Ruhr-University Bochum: Forschungszentrum Jülich, 2013.
[48] V. Gil, R.A. Strøm, L.J. Groven, M.-A. Einarsrud, $La_{28-x}W_{4+x}O_{54+3x/2}$ powders prepared by spray pyrolysis, J. Am. Ceram. Soc. 95 (2012) 3403–3407.
[49] S. Brunauer, P. Emmett, E. Teller, Adsorption of gases in multimolecular layers, J. Am. Ceram. Soc.60 (1938) 309–319.
[50] A. Kaiser, A. Prasad, S. Foghmoes, S. Ramousse, N. Bonanos, V. Esposito, Sintering process optimisation for multi-layer CGO membranes by in situ techniques, J. Eur. Ceram. Soc. 33 (2013) 549–556.
[51] P.Z. Cai, D.J. Green, a.G.L. Messing, Constrained densification of alumina/zirconia hybrid laminates, II: viscoelastic stress computation, J. Am. Ceram. Soc, 80, 19971940–1948.
[52] D.J. Green, O. Guillon, J. Rödel, Constrained sintering: a delicate balance of scales, J. Eur. Ceram. Soc. *28* (2008) 1451–1466.
[53] P.M. Raj, W.R. Cannon, Anisotropic shrinkage in tape-cast alumina: role of processing parameters and particle shape, J. Am. Ceram. Soc. 82 (1999) 2619–2625.
[54] M. Qiu, J. Feng, Y. Fan, N. Xu, Pore evolution model of ceramic membrane during constrained sintering, J. Mater. Sci. 44 (2009) 689–699.